

NUMERICAL STUDY ON MICRO-FRACTURE CHARACTERISTICS OF ROCK UNLOADING FAILURE UNDER HIGH STRESSES AND THE EXPLANATION FOR ROCK BURST

Yuezong YANG*, Anye LI

School of Science, Xi'an University of Architecture and Technology, Xi'an 710055, China

*corresponding author, yangyuezong@xauat.edu.cn

The micro-structure of rock essentially affects its macroscopic mechanical behaviors. To investigate the effect of micro-structure on the rock burst, an improved grain-based discretized virtual internal bond (GB-DVIB) model is developed. By the improved GB-DVIB model, different types of mineral grains and grain-boundaries can be generated effectively. A novel parameter calibration method, in which the scanning electron microscope, nano-indentation approach and conventional mechanical tests are utilized synthetically, is proposed. The single face unloading test is simulated to verify the ability of the improved GD-DVIB model to simulate the rock burst. The simulated results show that the the improved GB-DVIB model can simulate the intra- and inter-granular cracking and the main characteristics of the rock unloading failure process. The influence of the specimen size and the micro-structure on the rock burst proneness is investigated. As the height-to-thickness ratio decreases from large to small, the tensile failure characteristics weaken, while the shear failure characteristics enhance, manifested as the tensile-shear transition. With the increase of mineral grain size and heterogeneity, the rock burst proneness is stronger. Compared with the horizontal distribution of mineral grains, the vertical distribution can make the rock burst proneness stronger.

Keywords: grain-based method; unloading failure; micro-cracking process; rock burst.



Articles in JTAM are published under Creative Commons Attribution 4.0 International.
Unported License <https://creativecommons.org/licenses/by/4.0/deed.en>.
By submitting an article for publication, the authors consent to the grant of the said license.

1. Introduction

With the exploitation and utilization of underground space from shallow to deep, the rock burst is increasingly prominent and seriously threatens the safety of constructors and equipment. At present, the prediction and prevention of the rock burst is difficult to meet the requirements of engineering practice. The underlying reason is that the rock burst mechanism is highly complex and influenced by many factors. The influencing factors of the rock burst can be divided into two main categories, i.e., engineering geological factors and rock properties. The engineering geological factors contain in-situ stress, amplitude and frequency of dynamic disturbance load, unloading rate, temperature and so on. The rock properties contain strength, moisture content, brittleness, structural plane and so on. At the micro-scale, the rock is composed of the mineral grains. The types, content and properties of mineral grains essentially affect the properties of rock (Hofmann *et al.*, 2015). Therefore, to better understand the rock burst mechanism, it is necessary to investigate the rock burst from the point of micro-fracture at the mineral grain scale.

Many experimental studies have been conducted to investigate the micro-fracture characteristics of rock induced by the rock burst. Compared with the micro-fracture of the rock in compression experiments, the percentage of intra-granular cracks is higher and the fracture surface is rougher (He *et al.*, 2011) in rock burst experiments. Huang *et al.* (2012) utilized the triaxial unloading tests to investigate the rock burst, and concluded that with the increase of an unloading rate, the micro-fracture characteristics transform from an intra-granular shear fracture to an inter-granular tensile fracture gradually. Zhao *et al.* (2015) examined the composition

of the rock at the rock burst site, and found that the rock burst is more likely to occur in the hard-brittle rocks with a high degree of crystallization and the dense micro-structure. [Su *et al.* \(2019\)](#) studied the influence of mineral grain size on the rock burst, and found that the coarser mineral grain can make the rock burst proneness stronger. [Zheng and Wang \(2024\)](#) and [Jin *et al.* \(2024\)](#) investigated the influencing factors on the deformation and failure of porous coal, and found that the loading rate, borehole inclination and borehole diameter all have significant influences. These studies contribute to a deeper understanding of the rock burst from the perspective of micro-fracture. However, the rock burst is a violent dynamic fracture process, which brings some difficulties to the observation of the entire micro-fracture process. In this situation, the numerical simulation method is a powerful complement to further study the problem.

So far, many continuum-based numerical methods ([Manouchehrian & Cai, 2015](#)) have been adopted to investigate the rock burst. The stress and strain response can be calculated accurately by these methods. However, they have some limitation in fracture simulation, e.g., complicated fracture criterion and remeshing. Compared with these continuum-based methods, the discontinuum-based methods provide an effective and simple method for fracture simulation. The discontinuum-based methods discretize rocks into blocks or particles and connect them through springs or bonds, simulating the fracture process of rocks through the breaking of springs or bonds. The complicated 3D failure problem of material is transferred to the 1D bond rupture. Therefore, the issues of the complicated fracture criterion and re-meshing can be avoided in this method. The discrete element method (DEM) is a commonly used discontinuum-based method that can simulate the collapse of rock masses and the contact and rotation between rock blocks ([Cundall, 1988](#)). [Procházka \(2004\)](#) simulated the rock burst using both a hexagonal block and a particle DEM, and found that the hexagonal block DEM is more suitable for simulating crack initiation and propagation, while the particle DEM is more suitable for simulating dynamic failure processes. [Vacek *et al.* \(2008\)](#) used DEM to analyze the stress changes in the surrounding rock before and after tunnel excavation, and successfully simulated the block ejection phenomenon of the rock burst. [Zhu *et al.* \(2022\)](#) used DEM to study the influence of in-situ stress on the rock burst tendency and found that as the burial depth increases, the stress and released elastic strain energy increase, making the rock burst more likely to occur. However, due to the lack of theoretical relationship between macroscopic parameters and microscopic bond parameters, the calibration of microscopic bond parameters in DEM is inconvenient.

The discretized virtual internal bond (DVIB) ([Zhang, 2013](#)) model is another discontinuum-based method. This method considers a material to consist of bond cells. Each bond cell can take any geometry with any numbers of bonds, which makes it suitable to represent the micro-structure of geomaterials. Based on the ideal unit cell, the theoretical relationship between macroscopic parameters and microscopic bond parameters is established. Compared with the DEM, the microscopic bond parameters can be calibrated more conveniently in the DVIB model. The two-body potential adopted in DVIB only accounts for the normal interaction between two particles, which leads to an issue of fixed the Poisson ratio. To solve the issue, [Zhang *et al.* \(2014\)](#) proposed the Stillinger–Weber (SW) potential based DVIB (SW-DVIB) model. In this method, a modified SW potential, which is not only related to the normal deformation of bond, but also the bond angles, is embed in the DVIB. However, the realistic micro-structures of rock, e.g., the mineral grain and grain boundaries, have not been sufficiently considered in these DVIB methods. To simulate a microscopic fracture process of rocks more realistically, a grain-based DVIB (GB-DVIB) ([Yang & Zhang, 2022](#)) is developed to simulate the micro-structure at the mineral grain scale. A micro-structure generation method based on the Voronoi polygon has been proposed to more realistically represent micro-structure of rock. By this method, mineral grains and grain boundaries can be generated conveniently. The SW-DVIB is adopted to model the mineral grains, and a contact model considering the tension and shear is adopted to model the grain boundaries. However, the GB-DVIB model approximately assumes that the mechanical properties of different mineral grains are consistent.

In this study, the GB-DVIB model is improved. According to the observed types of mineral grains and the measured micromechanical properties, different mineral grains are assigned different mechanical parameters. To facilitate the application of the improved GB-DVIB model, a novel parameter calibration method is proposed. In this method, the scanning electron microscope (SEM), nano-indentation approach and conventional mechanical tests are utilized synthetically. The micro-fracturing process of granite samples in direct tension tests, uniaxial compression tests and confined compression tests are simulated. The simulated results show that the micro-fracture process, such as the inter-grain fracture and intra-grain fracture, is reproduced successfully. Then, the method is used to simulate rock burst. The three stages of the rock burst, i.e., several small grains ejecting, big fragment falling down and a lot of big fragments ejection, can be reproduced well. The effect of the height-to-thickness ratio and mineral grain size on the rock burst is investigated. The simulated results are basically consistent with the experimental results. The effect of micro-structure on the rock burst is investigated by the simulation of SFUT. The simulated results show that with the increase of mineral grain size and heterogeneity, the rock burst proneness is stronger. Compared with horizontal distribution of mineral grains, the vertical distribution can make the rock burst proneness stronger.

2. Grain-based DVIB model

2.1. Generation of micro-structure

Rock is a combination of mineral grains. Take the granite as an example, as shown in Fig. 1a, the main mineral grains contain the quartz, feldspar (plagioclase and potash feldspar) and biotite (Su *et al.*, 2019). The Voronoi polygon is highly similar to the micro-structure of rock (Li *et al.*, 2017). A micro-structure generation method based on the Voronoi polygon is proposed to more realistically represent micro-structure of rock. Based on the SEM images, the average mineral grain size and the percentages of different kinds of mineral grains are obtained, and then used as the key parameters to generate the micro-structure of rock by the Voronoi algorithm. Simply put, the employment of the Voronoi algorithm to generate micro-structure in the GB-DVIB model is based on the statistical averaging of real micro-structure in SEM images.

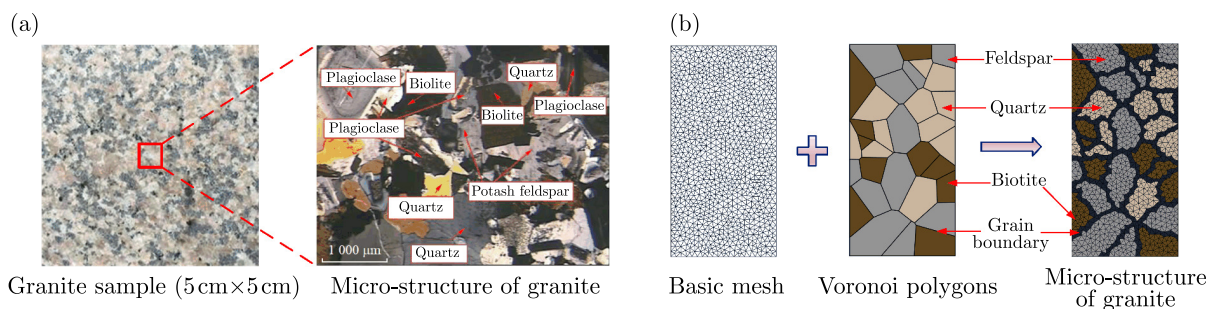


Fig. 1. Generation of micro-structures in GB-DVIB: (a) mineral grain composition of granite; (b) generation process of the micro-structure of granite.

The detailed micro-structure generation process of granite is shown in Fig. 1b. First of all, the basic bond cells and Voronoi polygons are generated by the code of GMesh and MATLAB, respectively. A polygon represents a mineral grain. The edges of polygons represent the grain boundaries. The mineral grain size and the mineral types can be set up according to the actual mineral grains. Different mineral grains are endowed with different mechanical properties. Then, the basic bond cells are covered by Voronoi polygons. If a bond cell is in a Voronoi polygons, the bond cell is defined as grain bond cells. While the bond cells which are cut by the edges of the Voronoi polygons are defined as the interface bond cells. By this method, different mineral grains and grain boundaries can be generated conveniently.

The degree of discretization and types of mesh can affect the calculation results of the GB-DVIB model. The GB-DVIB model is developed based on the DVIB model. The influences of the mesh size on the elastic modulus and the Poisson ratio of materials in the DVIB model is investigated in the previous study (Zhang, 2013). The research results indicate that with the decrease of the mesh size, the calculation error decreases. When the mesh is fine enough, the calculation error is close to zero. The influence of the mesh size on the calculation results of the DVIB model also applies to the GB-DVIB model. In the rock simulation of this study, the average size of the basic mesh is 0.25 mm. Through the verification, the mesh size meets the calculation accuracy requirements.

2.2. SW-DVIB model for mineral grain

The discretized virtual internal bond (DVIB) (Zhang, 2013) model is a developed lattice model by dispersing the continuous virtual internal bond (VIB) (Gao & Klein, 1998). It is composed of unit bond cells. The bond cells can take any geometry with finite micro-bonds, which make the DVIB suitable to represent the micro-structure of geomaterials. Compared with VIB, the individual behavior of every bond is considered in DVIB. Bond potentials are adopted to describe the bond mechanical behavior.

The Stillinger–Weber (SW) potential based DVIB (SW-DVIB) (Zhang *et al.*, 2014) is employed to model mineral grain. Compared with the traditional DVIB, the modified SW potential, which is not only related to the normal deformation of bond, but also the bond angles, is adopted to characterize the bond cell (Fig. 2a). The modified SW potential used for the rock fracture simulation (Zhang *et al.*, 2015) is

$$\Phi_2 = \frac{1}{2}Al_0^2(\tilde{r}_I - 1)^2, \quad \Phi_3 = \frac{1}{2}\lambda(\theta_{IJ} - \theta_{IJ0})^2, \quad (2.1)$$

where Φ_2 and Φ_3 are two- and three-body interactions, respectively; A and λ are material parameters, $A = 2V/[N(N-1)l_0^2] \cdot 3E/(1-2\mu)$ and $\lambda = V/[N(N-1)(N-2)] \cdot 9E(1-4\mu)/[2(1+\mu)(1-2\mu)]$; V is the volume of a bond cell; N is the number of bonds in a bond cell; E is the elastic modulus of material; μ is the Poisson ratio; l_0 is the bond length when undeformed; \tilde{r}_I is the normalized bond length, $\tilde{r}_I = r_{ij}/l_0$; θ_{IJ} is the bond angle subtended by the bond r_{ij} and r_{ik} in the current configuration, and θ_{IJ0} is the value in the reference configuration.

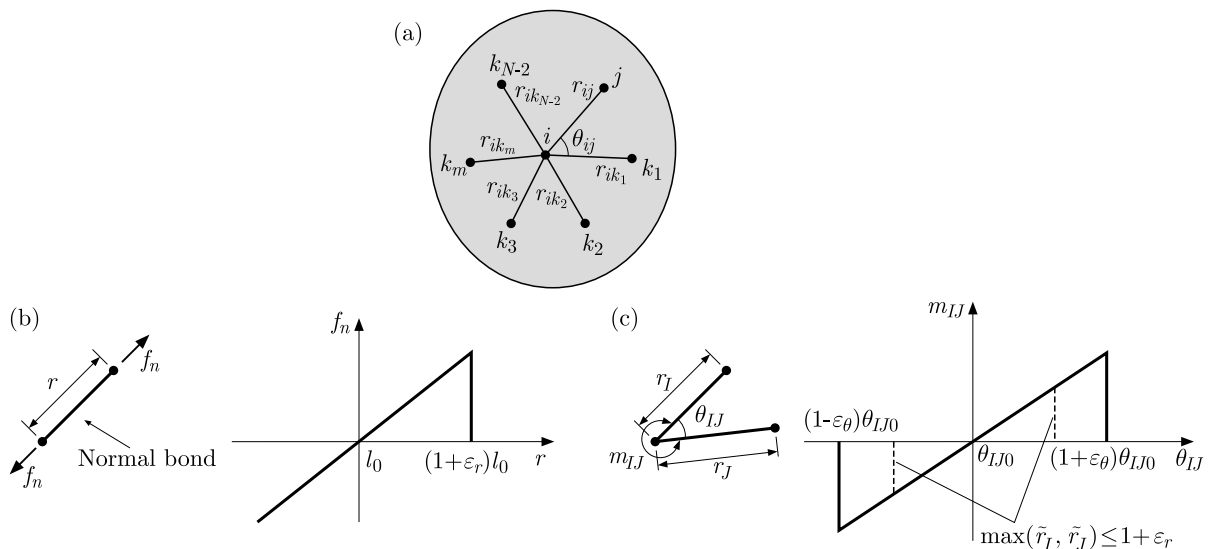


Fig. 2. Modeling mineral grains by SW-DVIB: (a) a bond cell with N particles; (b) normal bond force versus bond length; (c) bond moment versus bond angle.

According to (Zhang *et al.*, 2015), the constitutive relation (Figs. 2b and 2c) of SW-DVIB can be written as

$$f_n = \frac{\partial \Phi_2}{\partial r} = \begin{cases} Al_0(\tilde{r} - 1) & \text{if } \tilde{r} - 1 \leq \varepsilon_r, \\ 0 & \text{else,} \end{cases} \quad (2.2)$$

$$m_{IJ} = \frac{\partial \Phi_3}{\partial \theta_{IJ}} = \begin{cases} \lambda(\theta_{IJ} - \theta_{IJ0}) & \text{if } \max(\tilde{r}_I, \tilde{r}_J) \leq 1 + \varepsilon_r \text{ and } |\theta_{IJ} - \theta_{IJ0}| \leq \varepsilon_\theta, \\ 0 & \text{else,} \end{cases}$$

where f_n is the normal bond force, m_{IJ} is the bond moment, ε_r is the critical bond length strain, ε_θ is the critical bond angle strain.

2.3. Modeling grain boundaries

As shown in Fig. 3a, the bond cells cut by the grain boundaries are defined as interface bond cells. In the interface bond cells, the bonds cut by the grain boundaries are defined as interface bonds, while the other bonds are intact bonds. A contact model considering the tension and shear is adopted in these interface bonds. Before the rupture of the interface bonds, they are considered as intact bonds. The contact normal stress and shear stress of these interface bonds are calculated as

$$\sigma_n = \frac{f_{y'}}{A_c^b}, \quad \tau = \frac{f_{x'}}{A_c^b}, \quad (2.3)$$

where $[f_{x'}, f_{y'}]^T$ is the contact force vector of the interface bond in the local coordinate, $[f_{x'}, f_{y'}]^T = \mathbf{T}\Sigma\mathbf{f}$, \mathbf{T} is the coordinate transform matrix from the global coordinate to the local one, and \mathbf{f} is the internal force of interface bonds, A_c^b is the equivalent contact area of the interface bond (Fig. 3b), $A_c^b = A/N_{cra}$, A is the sectional area of the interface bond cell, N_{cra} is the number of interface bonds in the interface bond cell.

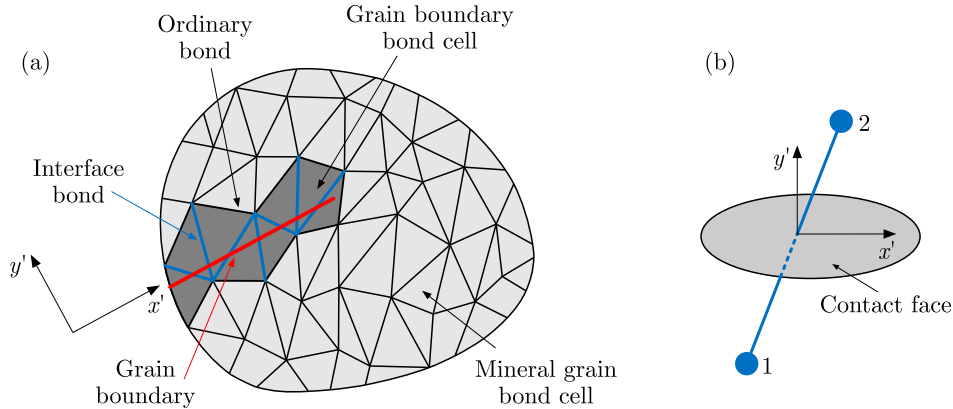


Fig. 3. Grain interface modeling: (a) interface bonds; (b) contact face adjunct to an interface bond.

Once the contact stress satisfied the failure criterion (tension failure or shear failure), the interface bond rupture. The failure criterion is

$$\sigma_n > \bar{\sigma}_n, \quad \tau > c + \sigma_n \cdot \tan \varphi, \quad (2.4)$$

where $\bar{\sigma}_n$ is the tensile strength of grain boundary, c is the cohesion, φ is the internal friction angle.

3. Parameter calibration

Parameter calibration is a key step in the application of numerical simulation methods. To facilitate the application of the improved GB-DVIB model, a novel parameter calibration

method is proposed. In this method, the scanning electron microscope (SEM), nano-indentation approach and conventional mechanical tests are utilized synthetically.

3.1. Procedure of parameter calibration

The macro-mechanical behaviors of rock are significantly influenced by the types, content and properties of mineral grains. The mineral composition and micro-structure of different rocks vary greatly. Take granite as an example, the procedure of parameter calibration in GB-DVIB is explained. SEM is adopted to analysis the main mineral composition and the average grain size (Zhang *et al.*, 2017). The main minerals of granite contain the quartz, felspar and biotite. The percentages of quartz, felspar and biotite are approximately 30 %, 45 %, and 25 %, respectively (Zhang *et al.*, 2017). The average grain size is 2.23 mm. According to the quantitative relationship between micro-bond parameters and macro-mechanical parameters in DVIB (Zhang, 2013), the mechanical parameters of mineral grains and grain boundaries obtained by the nano-indentation approach (Sun *et al.*, 2020) are used as the initial input parameters. The direct tension tests, uniaxial compression tests and confined compression tests are conducted to obtain the macro-mechanical parameters (Peng *et al.*, 2017a; 2017b). The macro-mechanical parameters include the Young modulus (E), tensile strength (σ_t), uniaxial compressive strength (UCS), and triaxial compressive strengths under different confining pressures.

With the initial input parameters, a series of direct tension tests, uniaxial compression tests and confined compression tests are simulated. The geometries of simulated granite samples are shown in Fig. 4. The height (H) and thickness (T) of the specimen are 100 mm and 50 mm, respectively. By comparing the simulated macro-mechanical behaviors with experimental results, the material parameters are adjusted. The process of parameter adjustment is as follows:

- 1) the Young modulus of granite (E) is used to calibrate the Young modulus of mineral grains (E_q , E_f , and E_b ; where the subscripts q , f , and b represent quartz, feldspar, and biotite, respectively) and the grain boundaries (E_{gb});
- 2) the tensile strength (σ_t) is used to calibrate the critical bond length strains of mineral grains (ε_{rq} , ε_{rf} , and ε_{rb}) and the tensile strength of grain boundary ($\bar{\sigma}_n$);
- 3) the UCS is used to calibrate the cohesion of the grain boundary (c) and the Poisson ratios (μ_q , μ_f , and μ_b), and the critical bond angle strain ($\varepsilon_{\theta q}$, $\varepsilon_{\theta f}$, and $\varepsilon_{\theta b}$) of mineral grains;
- 5) the triaxial compressive strengths under different confining pressures are used to calibrate the internal friction angle of the grain boundary (φ) and the normal and shear stiffness of the crack face (k_n and k_s).

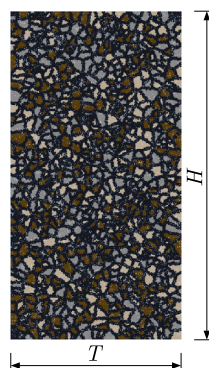


Fig. 4. Geomerty of simulated granite samples.

By repeating the process of parameter adjustment, once the adjusted input parameters can make the simulated results match the experimental results well, the adjusted input parameters can be taken as the calibrated ones. By the aforementioned procedure of parameter calibration, the material parameters are calibrated as

- quartz: $E_q = 20.26$ GPa, $\mu_q = 0.15$, $\rho_q = 2650$ kg/m³, $\varepsilon_{rq} = 2.4 \times 10^{-3}$, $\varepsilon_{\theta q} = 1.92 \times 10^{-3}$;
- feldspar: $E_f = 8.45$ GPa, $\mu_f = 0.2$, $\rho_f = 2600$ kg/m³, $\varepsilon_{rf} = 3.6 \times 10^{-3}$, $\varepsilon_{\theta f} = 3.06 \times 10^{-3}$;
- biotite: $E_b = 7.11$ GPa, $\mu_b = 0.3$, $\rho_b = 2600$ kg/m³, $\varepsilon_{rb} = 4.1 \times 10^{-3}$, $\varepsilon_{\theta b} = 3.28 \times 10^{-3}$;
- grain boundary: $E_{gb} = 7.11$ GPa, $\bar{\sigma}_n = 39.75$ MPa, $k_n = 10$ MPa, $k_s = 1$ kPa, $c = 45$ MPa, $\varphi = 28^\circ$.

3.2. Direct tension test

The simulated results of direct tension test are shown in Fig. 5. The simulated tensile strength is 10.51 MPa. Compared with the experimental tensile strength (10.1 MPa), the relative error is 4.06%. The simulated Young modulus is 33.75 GPa. Compared with the experimental Young modulus (35.5 GPa), the relative error is -4.93% . The simulated micro-fracture process shows that when the axial stress reaches 85% of the tensile strength, the inter-granular tensile cracks initiate from the center of the sample. With the increase of axial stress, a macroscopic main crack propagates horizontally. Finally, a horizontal macroscopic crack is formed in the middle of the sample. In the process, intra-granular and inter-granular cracks both have been observed. The inter-granular cracks play a predominant role in the tensile failure of rock. The simulated results agree well with the experimental observation (Peng *et al.*, 2017b).

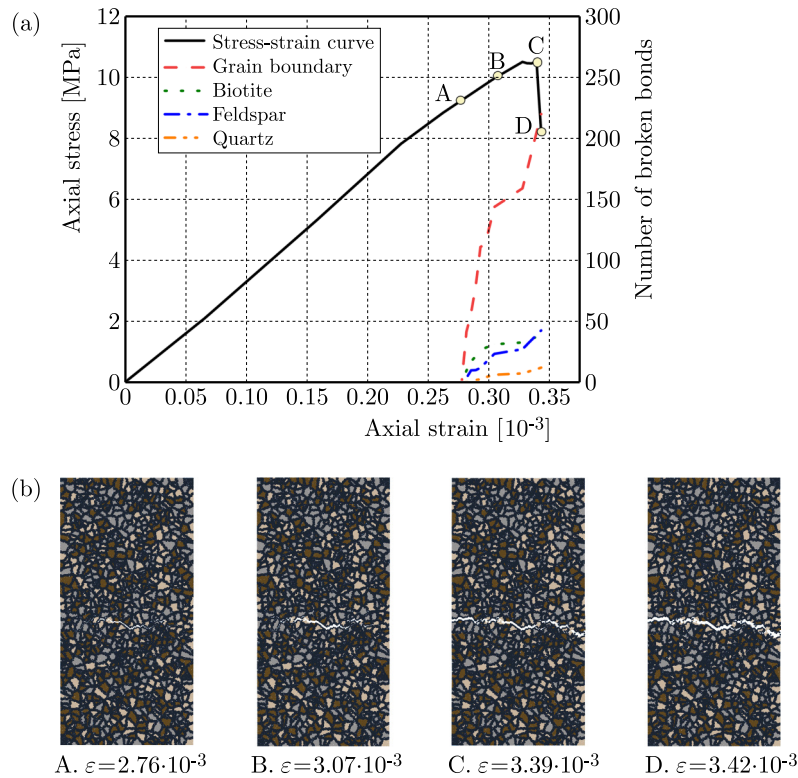


Fig. 5. Simulated results of direct tension tests: (a) stress-strain relationship and evolution of broken bonds; (b) micro-fracture process.

3.3. Uniaxial compression test

The simulated results of uniaxial compression test are shown in Fig. 6. The simulated UCS is 189.03 MPa. Compared with the experimental UCS (184.70 MPa), the relative error is 2.33%. The simulated micro-fracture process shows that when the axial stress reaches about 60% of UCS, the inter-granular cracks have been observed firstly. When the axial stress reaches about 70% of UCS, the intra-granular cracks occur. Due to the initiation, propagation and coalescence of micro-cracks, a macroscopic shear crack propagates from the lower right corner

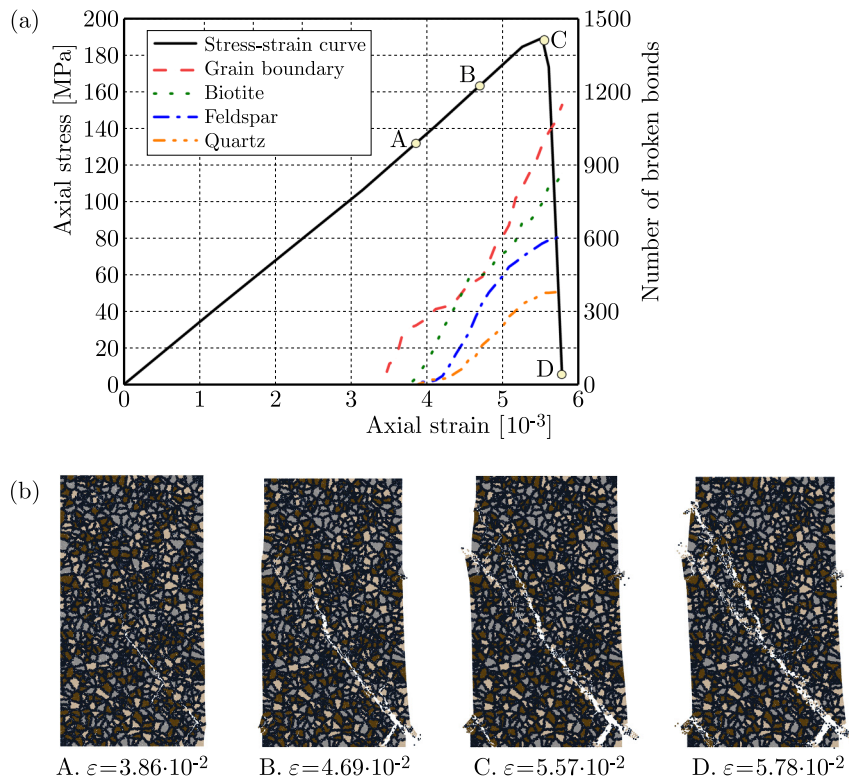


Fig. 6. Simulated results of uniaxial compression tests: (a) stress-strain relationship and evolution of broken bonds; (b) micro-fracture process.

of the sample to the upper left corner. Compared with the direct tension test, the final number of broken bonds and the percentage of intra-granular cracks in uniaxial compression test is larger. The simulation results are in good agreement with the experimental results (Peng *et al.*, 2017b).

3.4. Confined compression test

The simulated results of confined compression test are shown in Fig. 7. As shown in Fig. 7a, with the increase of the confined pressure, the strength of the granite sample increases. Because the friction of the crack face is considered in the improved GB-DVIB model, the residual strength

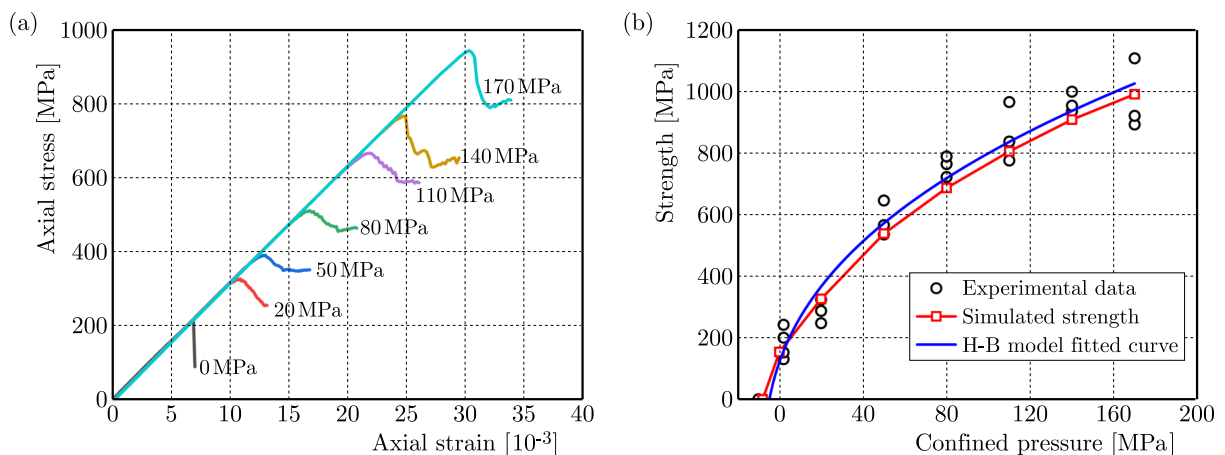


Fig. 7. Simulated results of confined compression tests: (a) stress-strain relationships with different confined pressures; (b) comparison between simulated strength with experimental one (Peng *et al.*, 2017b).

can be reflected well. As shown in Fig. 7b, the Hoek–Brown failure criterion is adopted to fit the experimental data. The fitted UCS and the material parameter m_i are 184.7 MPa and 23.2, respectively (Peng *et al.*, 2017b). The simulated strengths of samples under different confined pressures are almost corresponding to the fitted result. The comparison between the simulated and experimental results shows that the effect of confined pressure on triaxial strength can be reflected by the improved GB-DVIB model.

4. Simulation of rock unloading failure

Before the excavation of tunnel, the rock mass is in a quasi-static triaxial stress state. The excavation of the tunnel makes the rock mass to change from the triaxial stress state to the biaxial or uniaxial stress state, which induces the release of strain energy in rock mass to lead to the rock burst. Based on the evolution of the stress state during the rock burst, the single face unloading test (SFUT) (He *et al.*, 2012; Zhao & He, 2016) has been conducted to investigate the dynamic fracture process of rock during the rock burst.

The SFUT is conducted by a true triaxial testing system. At first, the original triaxial stress state is applied by triaxial loading. Then, one surface of the sample is unloaded abruptly to simulate the excavation (Fig. 8a). In the simulation, the SFUT is simplified as a two-dimensional plane strain problem, as shown in Fig. 8b. The height H of the sample is 150 mm, and the thickness T is 60 mm. A load-unloading path similar to experimental process is adopted. First, the lateral constraints of the left and right boundaries and the axial constraint of the low boundaries is fixed, and displacement loading is applied at the top of the specimen. When the axial stress reaches about 80 % of the UCS of the specimen, the constraint on the right side is suddenly released and the axial load continues to be applied until the final failure of the sample. The application of boundary conditions is completed through a MATLAB code. The calculation process of the main program is implemented by the Intel Parallel Studio solver on Microsoft's Visual Studio platform using the Fortran language. The materials parameters calibrated in Section 3 are adopted in the simulation.

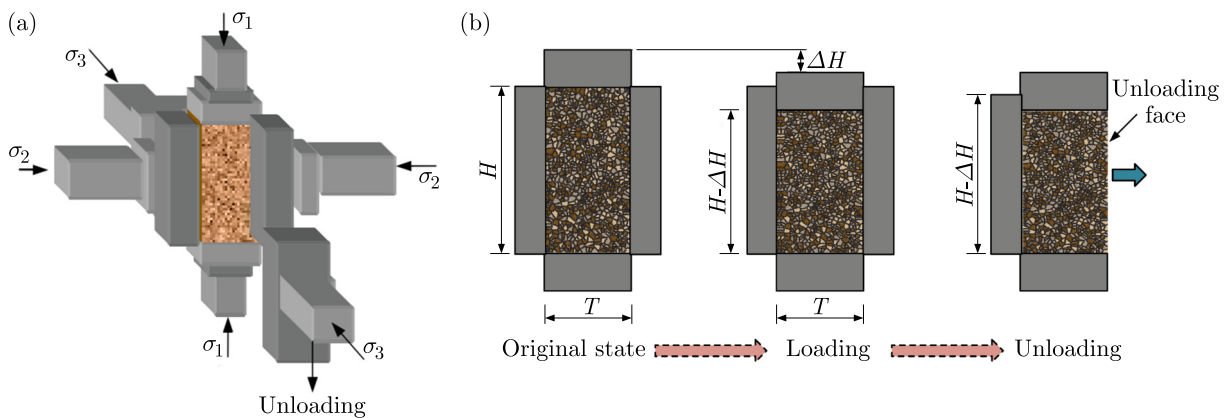


Fig. 8. Geometry and boundary conditions of SFUT: (a) schematic diagram of the SFUT (He *et al.*, 2012); (b) simplified loading-unloading process in simulation.

4.1. Rock failure process in SFUT

To examine the performance of the improved GB-DVIB model in simulating the fracture process of rock during the rock burst, the SFUT is simulated. The simulated results are shown in Figs. 9a and 9b. In the loading stage, the strain energy of the rock sample increases with the increase of axial displacement. In this stage, there are no broken bonds. The release of the constraint of the right boundary makes the strain energy release abruptly, which make several small grains eject from the unloading face. After the unloading point, the broken bonds have

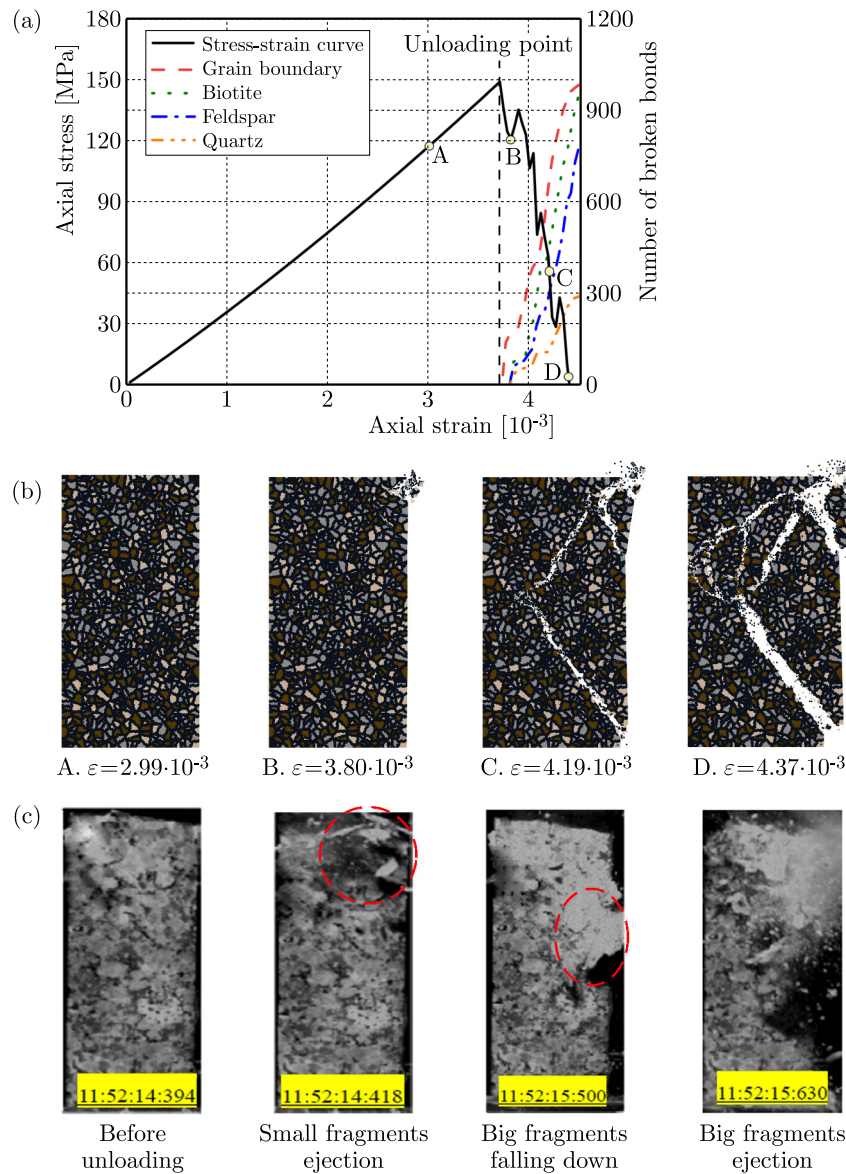


Fig. 9. Comparison between simulated SFUT and experimental results (a) simulated stress-strain relation and evolution of broken bonds; (b) simulated failure process; (c) experimental failure process.

been observed. Then, the application of axial displacement makes a big fragment fall down. Finally, a lot of big fragments eject from the unloading face, which leads to the ultimate failure of the rock sample. The similar failure process of a rock sample during the rock burst has been observed in the SFUT (He *et al.*, 2012), as shown in Fig. 9c. This indicates that the main characteristics of the rock burst process can be captured by the present method.

4.2. Effect of height-to-thickness ratios of specimen

The size effect of rock samples has a significant impact on their strength and failure mode. To investigate the size effect of rock samples on rock unloading failure, SFUTs with different height-to-thickness ratios (H/T) are simulated. In these tests, the H/T of granite sample varies from 5 to 2 with a fixed thickness of 30 mm. As shown in Fig. 10, when $H/T = 5$ and 4, the failure of the sample is mainly caused by splitting, and the tensile failure characteristics are obvious. When $H/T = 3$ and 2, shear cracks propagate from the top and bottom corners of the unloading surface of the specimen, and the shear failure characteristics are obvious. Therefore, as the H/T

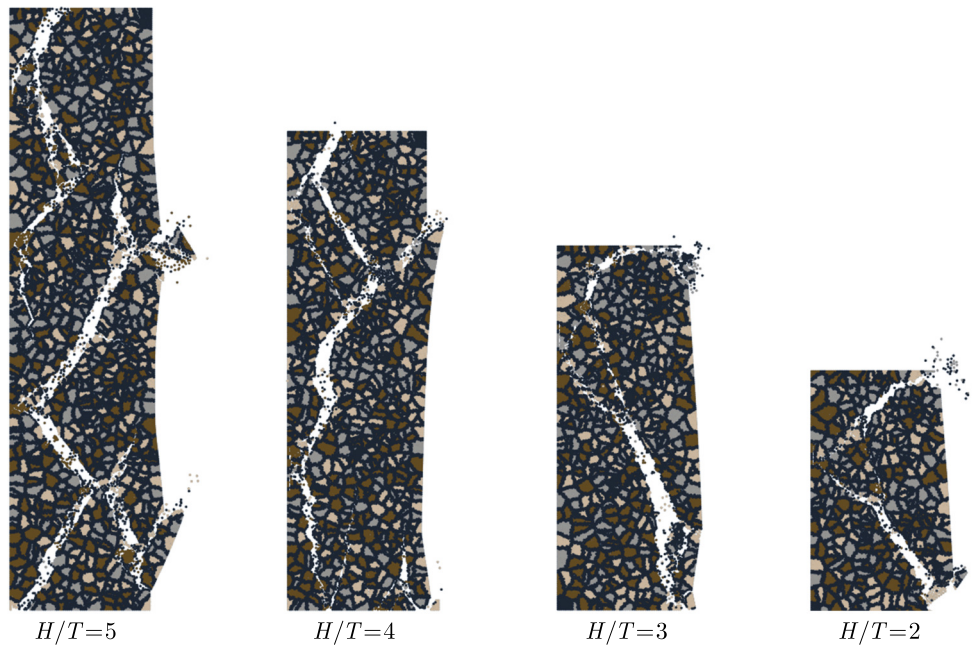


Fig. 10. Simulated fracture patterns of the samples with different H/T .

decreases from large to small, the tensile failure characteristics weaken, while the shear failure characteristics enhance, manifested as the tensile-shear transition. The failure regular pattern is basically consistent with the experimental observation.

The height-to-thickness ratio effect of rock samples is mainly caused by the end friction effect and the number of defects. When the rock sample is short, the stress distribution is relatively uniform due to the end effect, and the sample is basically in a three-dimensional stress state as a whole. In this case, the lateral displacement of the specimen is not significant due to the constraint at the ends, and the failure of the specimen exhibits shear failure. As the height of the specimen increases, the end constraints have little effect on the middle part of the sample, the stress in the middle of the rock sample gradually transitions from a three-dimensional stress state to a one-dimensional stress state. At this point, there will be a significant lateral displacement in the middle of the sample, leading to a significant increase in the tensile stress and resulting in tensile failure. At the same time, as the height of the sample increases, the defects inside the rock intensifies. During the compression process of the specimen, there will be more initiation points and ultimately more complex failure modes.

4.3. Effect of mineral grain size

The mineral grain size has a significant impact on the macroscopic mechanical behavior of rocks. The effect of the mineral grain size on the rock burst is analyzed by four cases with different average mineral grain diameters, namely $D_g = 2.0, 2.5, 3.0,$ and 3.5 mm. The simulated results show that with an increase of the mineral grain size, the rock burst is more violent. As shown in Fig. 11, when $D_g = 2.0$ mm, the upper right corner of the specimen was fractured and ejected due to the local stress concentration, and a main crack runs through the lower right corner at an angle of about 60 degrees to the upper left corner. With an increase of the mineral grain size, the degree of fragmentation and dynamic characteristics of the sample have intensified. When $D_g = 3.5$ mm, the right part of the sample splits and pops out as a whole, and the rock is broken into many small pieces in the middle of the sample. Ultimately, a large V-shaped crater is formed. It should be noted that the similar experimental results have also been obtained by the physical model test (Su *et al.*, 2019).

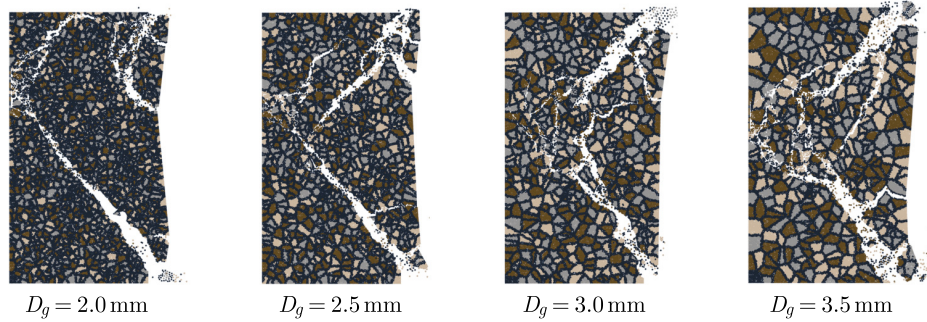


Fig. 11. Failure patterns of granite samples with different grain sizes.

The influence of the mineral grain size on the rock burst is essentially determined by the non-uniformity of the mineral grain distribution. When the mineral grain size is large, the non-uniformity of the mineral grain distribution becomes stronger. During the loading process, the rock is more prone to tensile stress concentration and local accumulation of elastic strain energy. When the local elastic strain energy exceeds the rock bearing limit, it will cause local failure of the specimen, that is, the dissipation of energy is relatively random and dispersed in the spatial and temporal distribution. In this case, the failure of the specimen tends to occur through dynamic failure, namely severe rock ejection phenomenon. When the mineral grain size is small, the non-uniformity of mineral grain distribution becomes weaker. During the loading process, due to the relatively uniform distribution of stress field inside the specimen, the concentration of local tensile stress and elastic strain energy is less likely to occur. As the load increases, the specimen will gradually swell, break, and slide outward, with concentrated and continuous damage locations.

4.4. Effect of mineral grain heterogeneity

The non-uniformity of mineral grains can cause uneven stress distribution, which in turn affects the macroscopic mechanical behavior of rocks. To investigate the effect of mineral grain heterogeneity on the rock burst, two cases with different random distribution of mineral grains are simulated. The average mineral grain diameters in these two cases are both 2.5 mm. The simulated failure patterns are shown in Fig. 12. When mineral grain heterogeneity is strong, two shear cracks initiate from the upper and lower parts of the unloading surface and propagate towards the middle of the specimen, ultimately leading to the overall failure of the specimen and forming a V-shaped crater. When mineral grain heterogeneity is weak, the sample failure is concentrated in the upper right part of the sample, manifested as local splitting of the sample. Therefore, as the mineral grain heterogeneity decreases, the failure area decreases, and the failure pattern exhibits the shear-tension transition. Compared with the homogeneous sample, the rock burst proneness of a heterogeneous sample is stronger.

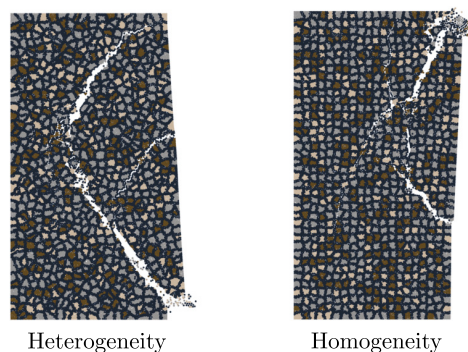


Fig. 12. Failure patterns of granite samples with different gain randomness.

The effect of mineral grain heterogeneity on the rock burst can be further explained by the direction distribution of a mineral grain interface. As shown in Fig. 12, the mineral grain heterogeneity can significantly affect the direction distribution of mineral grain interfaces. When the mineral grain heterogeneity is strong, the direction of mineral grain interfaces is random. However, when the mineral grain heterogeneity is weak, the direction of mineral grain interfaces tends to be vertical and horizontal. Overall, the mechanical properties of mineral grain interfaces are weaker than those of mineral particles. The directional distribution of mineral grains has a significant effect on the failure of rock samples. When the mineral grain heterogeneity is strong, the randomly distributed mineral grain interfaces will fracture and penetrate, ultimately forming two macroscopic shear cracks. When the mineral grain heterogeneity is weak, the vertical mineral grain interfaces are more likely to fracture and ultimately result in splitting failure of the sample.

4.5. Effect of mineral grain directionality

Mineral grains in sedimentary rocks have a certain directionality during the sedimentation process. The directionality of mineral grain greatly influences the anisotropic behavior of the rock sample (Ghazvinian *et al.*, 2014). To investigate the effect of mineral grain directionality on the rock burst, two typical distributions, namely vertical and horizontal distribution, are analyzed. The average mineral grain diameters in the two cases are both 3.0 mm. The simulated failure patterns are shown in Fig. 13. When the mineral grains are arranged vertically, it is discovered that two shear cracks begin at the top and bottom of the unloading surface and move towards the centre of the specimen. This finally causes the specimen to fail completely and leaves a V-shaped crater. The sample failure is centred in the top right portion of the sample and appears as localised splitting when the mineral grains are spread horizontally. The rock burst proneness of the rock sample with vertically distributed mineral grains is stronger than that with horizontally distributed mineral grains.

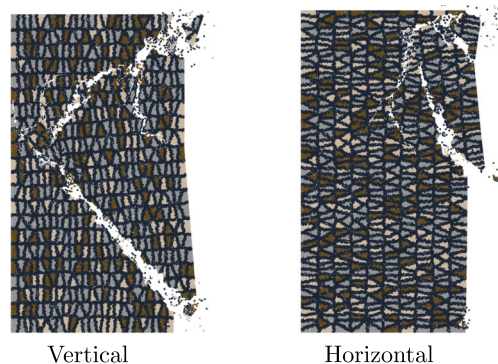


Fig. 13. Failure patterns of granite samples with different grain directionality.

The effect of mineral grain directionality on the rock burst can also be explained by the direction distribution of a mineral grain interface. As shown in Fig. 13, when the mineral grains are distributed vertically, the long side of mineral grains is in the vertical direction, and the short side of mineral grains is in the horizontal direction. In contrast, when the mineral grains are distributed horizontally, the long side and short side of the mineral grains are in the horizontal and vertical directions, respectively. Under the vertical compression load, the vertical interface of mineral particles will undergo tensile failure under the lateral expansion caused by compression, while the horizontal interface will undergo compression without failure. For the vertically distributed mineral grains, the failure of the long side of the mineral grains in the vertical direction can lead to a violent failure of the sample. While, for the horizontally distributed mineral grains, the failure of the short side of the mineral grains in the vertical direction causes weaker failure than vertically distributed mineral grains.

5. Conclusions

The GB-DVIB model is improved to investigate how the micro-structure affects the rock burst. By the improved GB-DVIB model, different types of mineral grains and grain-boundaries can be generated effectively. A novel parameter calibration method, in which the SEM, nano-indentation approach and conventional mechanical tests are utilized synthetically, is proposed. The SFUT is simulated to verify the ability of the improved GD-DVIB to simulate the rock burst. The simulated results show that the improved GB-DVIB model can simulate the intra- and inter-granular cracking and the rock burst process, i.e., small grains ejection, big fragments fall down and a lot of big ejection fragments. The influence of the sample size, the mineral grain size, heterogeneity and distribution directionality on rock unloading failure are investigated.

With the decrease of height-to-thickness ratio of specimen, the rock burst is more violent, and the fracture pattern exhibits the tensile-shear transition. This phenomenon is caused by end effects. With the increase of the mineral grain size, the rock burst is more violent. The underlying reason is that when the mineral grain size is large, the non-uniformity of mineral grain distribution becomes stronger. When the mineral grain heterogeneity is strong or the mineral grains are distributed vertically, the rock burst proneness is stronger. This is because when the mineral grain heterogeneity is strong, the direction of mineral grain interfaces is random, which is more likely to cause shear cracks to occur. While, when the mineral grain heterogeneity is weak, the direction of mineral grain interfaces tends to be vertical and horizontal, which is more likely to cause tensile cracks to occur. For the vertically and horizontally distributed mineral grains, the long and short sides of the mineral grains are in the vertical direction, respectively. The failure of more vertical grain interfaces in rock samples with vertically distributed grains results in a stronger tendency for the rock burst.

In this study, we adopted the Voronoi polygons to generate the micro-structure of rocks. Although the Voronoi polygons can reflect the main characteristics of the rock micro-structure, this is still a statistical averaging method. The micro-structure of rocks obtained through SEM images cannot be fully projected into the numerical model. In future research, we will attempt to generate more realistic micro-structure by projecting the SEM images into the numerical model.

Acknowledgments

This work is supported by the China Postdoctoral Science Foundation (no. 2023MD744236), the Natural Science Basic Research Program of Shaanxi (no. 2024JC-YBQN-0061), the Postdoctoral Research Project of Shaanxi Province (no. 2023BSHEDZZ270), the Special Scientific Research Plan Project of Education Department of Shaanxi Provincial Government (no. 23JK0509), and the Innovation and Entrepreneurship Projects for College Students (no. S202310703047).

References

1. Cundall, P.A. (1988). Formulation of a three-dimensional distinct element model – Part I. A scheme to detect and represent contacts in a system composed of many polyhedral blocks. *International Journal of Rock Mechanics and Mining Sciences & Geomechanics Abstracts*, 25(3), 107–116. [https://doi.org/10.1016/0148-9062\(88\)92293-0](https://doi.org/10.1016/0148-9062(88)92293-0)
2. Gao, H. & Klein, P. (1998). Numerical simulation of crack growth in an isotropic solid with randomized internal cohesive bonds. *Journal of the Mechanics and Physics of Solids*, 46(2), 187–218. [https://doi.org/10.1016/S0022-5096\(97\)00047-1](https://doi.org/10.1016/S0022-5096(97)00047-1)
3. Ghazvinian, E., Diederichs, M.S., & Quey, R. (2014). 3D random Voronoi grain-based models for simulation of brittle rock damage and fabric-guided micro-fracturing. *Journal of Rock Mechanics and Geotechnical Engineering*, 6(6), 506–521. <https://doi.org/10.1016/j.jrmge.2014.09.001>

4. He, M., Nie, W., Zhao, Z., & Cheng, C. (2011). Micro- and macro-fractures of coarse granite under true-triaxial unloading conditions (in Chinese). *Mining Science and Technology*, 21(3), 389–394. <https://doi.org/10.1016/j.mstc.2011.05.016>
5. He, M., Xia, H., Jia, X., Gong, W., Zhao, F., & Liang, K. (2012). Studies on classification, criteria and control of rockbursts. *Journal of Rock Mechanics and Geotechnical Engineering*, 4(2), 97–114. <https://doi.org/10.3724/SP.J.1235.2012.00097>
6. Hofmann, H., Babadagli, T., Yoon, J.S., Zang, A., & Zimmermann, G. (2015). A grain based modeling study of mineralogical factors affecting strength, elastic behavior and micro fracture development during compression tests in granites. *Engineering Fracture Mechanics*, 147, 261–275. <https://doi.org/10.1016/j.engfracmech.2015.09.008>
7. Huang, D., Tan, Q., & Huang, R. (2012). Study of micro-mesoscopic characteristics of marble fracture surface and correlation with unloading rock mass strength under high stress and unloading (in Chinese). *Rock and Soil Mechanics*, 33(Supp. 2), 7–15.
8. Jin, X., Zheng, J., Hua, S., & Tong, X. (2024). Influencing factors of deformation and failure of porous coal under conventional loading. *Facta Universitatis, Series: Mechanical Engineering*. <https://doi.org/10.22190/FUME240304036J>
9. Li, X.F., Li, H.B., & Zhao, J. (2017). 3D polycrystalline discrete element method (3PDEM) for simulation of crack initiation and propagation in granular rock. *Computers and Geotechnics*, 90, 96–112. <https://doi.org/10.1016/j.compgeo.2017.05.023>
10. Manouchehrian, A. & Cai, M. (2015). Simulation of unstable rock failure under unloading conditions. *Canadian Geotechnical Journal*, 53(1), 22–34. <https://doi.org/10.1139/cgj-2015-0126>
11. Peng, J., Wong, L.N.Y., & Teh, C.I. (2017a). Influence of grain size heterogeneity on strength and microcracking behavior of crystalline rocks. *Journal of Geophysical Research: Solid Earth*, 122(2), 1054–1073. <https://doi.org/10.1002/2016JB013469>
12. Peng, J., Wong, L.N.Y., Teh, C.I., & Li, Z. (2017b). Modeling micro-cracking behavior of Bukit Timah granite using grain-based model. *Rock Mechanics and Rock Engineering*, 51(1), 135–154. <https://doi.org/10.1007/s00603-017-1316-x>
13. Procházka, P.P. (2004). Application of discrete element methods to fracture mechanics of rock bursts. *Engineering Fracture Mechanics*, 71(4–6), 601–618. [https://doi.org/10.1016/S0013-7944\(03\)00029-8](https://doi.org/10.1016/S0013-7944(03)00029-8)
14. Su, G., Chen, G., Hu, X., Mei, S., & Huang, X. (2019). Experimental study on influence of granite grain size on rockburst (in Chinese). *Explosion and Shock Waves*, 39(12), 66–77. <http://dx.doi.org/10.11883/bzycj-2018-0419>
15. Sun, C., Li, G., Gomah, M.E., Xu, J., & Rong, H. (2020). Meso-scale mechanical properties of mudstone investigated by nanoindentation. *Engineering Fracture Mechanics*, 238, Article 107245. <https://doi.org/10.1016/j.engfracmech.2020.107245>
16. Vacek, J., Vacek, J., & Chocholoušová, J. (2008). Rock burst mechanics: Insight from physical and mathematical modelling. *Acta Polytechnica*, 48(6), 38–44. <https://doi.org/10.14311/1071>
17. Yang, Y. & Zhang, Z. (2022). Micro-fracture simulation of rock under unloading condition by grain-based discretized virtual internal bond method. *International Journal of Applied Mechanics*, 14(1), Article 2250001. <https://doi.org/10.1142/S1758825122500016>
18. Zhang, F., Guo, H., Zhao, J., Hu, D., Sheng, Q., & Shao, J. (2017). Experimental study of micro-mechanical properties of granite (in Chinese). *Chinese Journal of Rock Mechanics and Engineering*, 36(2), 3864–3872.
19. Zhang, Z. (2013). Discretized virtual internal bond model for nonlinear elasticity. *International Journal of Solids and Structures*, 50(22–23), 3618–3625. <https://doi.org/10.1016/j.ijsolstr.2013.07.003>
20. Zhang, Z., Chen, Y., & Zheng, H. (2014). A modified Stillinger–Weber potential-based hyperelastic constitutive model for nonlinear elasticity. *International Journal of Solids and Structures*, 51(7–8), 1542–1554. <https://doi.org/10.1016/j.ijsolstr.2014.01.003>
21. Zhang, Z., Yao, Y., & Mao, X. (2015). Modeling wave propagation induced fracture in rock with correlated lattice bond cell. *International Journal of Rock Mechanics and Mining Sciences*, 78, 262–270. <https://doi.org/10.1016/j.ijrmms.2015.06.006>

22. Zhao, F. & He, M.C. (2016). Size effects on granite behavior under unloading rockburst test. *Bulletin of Engineering Geology and the Environment*, 76(3), 1183–1197. <https://doi.org/10.1007/s10064-016-0903-5>
23. Zhao, K., Zhao, H., & Jia, Q. (2015). An analysis of rockburst fracture micromorphology and study of its mechanism. *Explosion and Shock Waves*, 35(6), 913–918. [https://doi.org/10.11883/1001-1455\(2015\)06-0913-06](https://doi.org/10.11883/1001-1455(2015)06-0913-06)
24. Zheng, J. & Wang, L. (2024). Experimental study on creep loading of porous coal under different influencing factors. *Facta Universitatis, Series: Mechanical Engineering*, 22(1), 153–163. <https://doi.org/10.22190/FUME231205011Z>
25. Zhu, B., Fan, J., Shi, X., Liu, P., & Guo, J. (2022). Study on rockburst proneness of deep tunnel under different geo-stress conditions based on DEM. *Geotechnical and Geological Engineering*, 40(3), 1373–1386. <https://doi.org/10.1007/s10706-021-01969-8>

*Manuscript received August 18, 2024; accepted for publication January 8, 2025;
published online March 1, 2025.*